Theory of doping properties of Ag acceptors in ZnO

O. Volnianska,[1] P. Boguslawski,[1,2] J. Kaczkowski,[3] P. Jakubas,[1] A. Jezierski,[3] and E. Kaminska[4]
[1]*Institute of Physics, PAS, al. Lotnikow 32/46, 02-668 Warsaw, Poland*
[2]*University of Bydgoszcz, ul. Chodkiewicza 30, 85-064 Bydgoszcz, Poland*
[3]*Institute of Molecular Physics, PAS, ul. M. Smoluchowskiego 17, 60-179 Poznan, Poland*
[4]*Institute of Electron Technology, al. Lotników 32/46, 02-668 Warsaw, Poland*
(Received 10 April 2009; revised manuscript received 22 November 2009; published 22 December 2009)

Doping properties of Ag in ZnO were analyzed by first-principles calculations within both the local-density and generalized gradient approximations. The ionization energy of Ag_{Zn}, about 0.2 eV, is comparable to that of the commonly used group-V acceptors, and is lower than that of two other I^B species, Cu and Au. Formation energy of Ag in the favorable O-rich conditions is 0.85 eV, which corresponds to the solubility limit of about 10^{18} cm^{-3} at 700 °C. Formation of Ag-rich second phases is predicted for high Ag concentrations. Energetics of the onset of this process is analyzed and Ag_{Zn} display a tendency to form aggregates of AgO with the wurtzite structure. Formation of such nanoinclusions is shown to affect the lattice constant of ZnO:Ag. Two "wrong" incorporation channels, i.e., at the interstitial sites and at the oxygen sites as Ag_O, are predicted to be nonefficient due to the high formation energies. The calculated magnetic coupling between Ag ion reveals an unexpected dependence on the Ag-Ag distance; the interaction between the nearest-neighbor Ag_{Zn} pair vanishes while that for the more distant pairs is weakly ferromagnetic.

DOI: 10.1103/PhysRevB.80.245212 PACS number(s): 71.55.Gs, 61.72.sh, 71.15.Mb

I. INTRODUCTION

ZnO, an II-VI oxide semiconductor, is a promising material for various technological applications, especially for optoelectronic light-emitting devices in the visible and ultraviolet range of the electromagnetic spectrum.[1,2] However, stable and reproducible *p*-type materials with satisfactory concentrations and high mobilities remain a challenging problem. The most often studied dopants are group-V atoms: N,[1,2] P,[3] As,[4] and Sb.[5,6] As an alternative, group-I dopants were proposed.[7–16] This comprises group-I^A Li, Na, and K, which were predicted to be shallow acceptors.[7] Indeed the *p* conductivity was observed both in ZnO:Li (Ref. 9) and in ZnO codoped with Li and N.[10] The relatively low hole concentrations of about 10^{16} cm^{-3} (Refs. 9–11) may be due to the fact that group-I^A species have a tendency to be incorporated as interstitial donors rather than substitutional acceptors.[7,12] Calculations of Ref. 8 also showed that group-I^B Ag is expected to be an efficient acceptor while Cu and Au are predicted to be deeper and thus less effective. Experimentally, energy levels of Cu and Ag are not conclusively determined yet. Early data situated the acceptor levels of Cu (Ref. 17) and Ag (Ref. 18) about 0.2 eV below the bottom of the conduction band. This value for Cu was used in Ref. 19 to interpret photoluminescence spectra. More recent measurements situated acceptor levels of both Ag and Cu about 0.3 eV above the top of the valence band.[20] The presence of Cu often leads to the copper-related green luminescence.[21] Transport measurements showed that introduction of Cu into ZnO, which as a rule is *n* type, leads to compensation displayed by the increased resistivity of samples.[22,23] Finally, growth of *p*-type ZnO:Cu was recently reported.[24] Turning to Ag, recent photoluminescence data indicated that the ionization energy of Ag is 0.246 eV.[25] In parallel, Kang *et al.*[13] reported *p* conductivity in Ag-doped ZnO. Subsequent works showed that hole concentrations strongly depend on the conditions of growth and annealing,[14–16] and the highest concentrations reported exceed 10^{18} cm^{-3}.[16]

Theoretically, it is recognized[26–29] that the difficulties in obtaining *p*-ZnO are related with several factors, the most important of which are limited solubility of a dopant, compensation by native donors, and nonintentional incorporation of hydrogen that is a shallow donor.[30] The role of these effects critically depends on the conditions of growth, which can vary from O rich to O poor. In fact, for given growth conditions the solubility of a substitutional dopant depends on the sublattice on which it resides. For example, incorporation of N on the O sublattice is more efficient in the O-poor conditions while the solubility of dopants substituting Zn, such as group-I^A atoms studied here, is higher in the opposite O-rich limit. Importantly, the O-rich conditions also strongly suppress the compensation by native donors.[26–29] Thus, usage of acceptors substituting Zn-rich and the O-rich conditions should optimize their doping efficiency because of both the increased solubility and the reduced intrinsic compensation. Previous studies[7–11,13–16] of group-I acceptors were partially motivated by this observation.

This work reports the results of theoretical studies of the doping efficiency of Ag and is organized as follows. The methodology is presented in Sec. II. Next, in an ideal case, doping efficiency of a substitutional impurity is determined by its solubility and ionization energy, which are evaluated in Sec. III. The calculated ionization energy of Ag is 0.4 eV, which is close to that of the commonly used group-V acceptors. The calculations were extended to two other group-I^B species, Cu and Au but their ionization energies are higher that of Ag, and thus a more detailed study of their doping properties was not performed. In practice, apart from the compensation by native defects that is not discussed here, there are several effects that can limit doping efficiency. In particular, in Sec. IV we analyze the onset of formation of AgO nanoinclusions with the wurtzite structure by examining the energetics of formation of small aggregates contain-

ing a few Ag_{Zn} ions. Two channels of Ag incorporation at the "wrong" sites, namely, the incorporation as an interstitial Ag_i donor and as an Ag_O "antisite," are examined in Secs. V and VI, respectively. The impact of Ag on the lattice constant of ZnO in the context of experimental data is discussed in Sec. VII.[13–15] Finally, magnetic coupling between Ag ions is examined in Sec. VIII.

II. COMPUTATIONAL TECHNIQUE

Calculations based on the density-functional theory were performed using both the local-density approximation[31] (LDA) and the generalized gradient approximation[32,33] (GGA). This is because typically the former approximation, LDA, underestimates the lattice constant and overestimates cohesive energies relative to the experimental values while the opposite is true for GGA. In other words, the results of the two methods bracket the experimental values. As we show, (Zn,Ag)O confirms this rule. Errors in the cohesive energies, i.e., in the strength of a given type of bond, lead to the errors in the formation energies of dopants and defects. Consequently, one can expect that an average of the LDA and GGA formation energies is more reliable than the LDA or GGA value itself. Considering the band structure we note that both approximations largely underestimate the band gap of ZnO. However, this issue, critical when considering donors, has a negligible influence on energies of acceptor levels that are derived from the valence states.

Finally, the energy of d(Zn) states within both LDA and GGA is too high, which results in their overhybridization with the p(O) states from the top of the valence band. The use of LDA+U approach[34] would decrease both hybridization and the energy of the valence-band top. In the studied case of I^B acceptors in ZnO, the +U corrections should consistently be applied to all the involved d orbitals but their impact is expected to be marginal because of the shallow character of the considered acceptors and thus were neglected. To verify this assumption we have calculated electronic structure of ZnO:Ag using both GGA and GGA+U methods. For Zn, the value proposed in Ref. 35, U =4.7 eV, was used. For Ag we assumed the same value as for the recently studied Cu, i.e., U=1 eV. This value is small but it leads to a good agreement with experiment.[36] The small value of U for Cu also agrees with the conclusions of Ref. 37, where it is pointed out that there is no experimental evidence of the strong correlations for 3d electrons in Cu. The results obtained with this choice show that, as expected, inclusion of +U corrections does not significantly alter the calculated properties of Ag. More specifically, in the energy window of 0.5 eV in the vicinity of the top of the valence band which is of main interest from the point of view of doping properties, inclusion of +U for Zn only affects eigenenergies of ZnO:Ag by about 0.05 eV. The subsequent inclusion of U for Ag does not change them to within 0.01 eV, which is the accuracy of the method, thus justifying our neglect of +U corrections.

The calculations were performed using two codes: QUANTUM-ESPRESSO code[38] and Vienna *ab initio* simulation package (VASP) (Ref. 39) with the projector augmented wave method.[40] Both codes are based on the plane-wave basis set, and, as demonstrated by a careful check, they lead to the same results within the accuracy expected from LDA/GGA. Both codes were used in Secs. III and IV, QUANTUM ESPRESSO in Secs. V–VII and VASP in Sec. VIII. The cutoff energy of 408 eV for the plane-waves' expansion and 3265 eV for the electronic charge density was found to be sufficient to obtain convergent results in QUANTUM-ESPRESSO code and 520 eV in VASP. Ultrasoft Vanderbilt pseudopotentials[41,42] included the 3d orbitals of Zn and Cu, 4d orbitals of Ag, and 5d of Au as valence states. Methfessel-Paxton smearing method[43] with the smearing width of 0.136 eV has been used for obtaining partial occupancies. Ionic positions were optimized until the forces acting on ions were smaller than 0.02 eV/Å. To study the impurities, large unit cells with up to 128 atoms were employed, and the Brillouin-zone summations were performed using the Monkhorst-Pack scheme[44] with a $2\times2\times2$ k-point mesh. The used k-point grids were $8\times8\times8$ for metal Zn and Ag, and $12\times12\times6$ for w-ZnO and w-AgO.

III. SUBSTITUTIONAL Cu_{Zn}, Ag_{Zn}, AND Au_{Zn}

The formation energy[45] of Ag_{Zn} in the neutral $q=0$ charge state is

$$E_{form}(q=0) = E(\mathrm{ZnO{:}Ag_{Zn}}) - E(\mathrm{ZnO}) + \mu(\mathrm{Zn}) - \mu(\mathrm{Ag}), \tag{1}$$

where the first two terms on the right-hand side are the total energy of the supercell with and without the impurity, respectively. μ is the chemical potential of Zn or Ag, which depends on the conditions of growth. Thermodynamic equilibrium requires that $\mu(\mathrm{Zn})+\mu(\mathrm{O})=\mu(\mathrm{Zn\ bulk})+\mu(\mathrm{O_2})+\Delta H_f(\mathrm{ZnO})$, where ΔH_f(ZnO) is the heat of formation of ZnO at zero temperature (ΔH_f is negative for stable compounds). $\mu(O_2)$ is the binding energy of O_2. In the metal-rich conditions μ(Zn) is equal to the cohesive energy E_{coh} of bulk metal. In the O-rich conditions, relevant for the present work, $\mu(\mathrm{Zn})=\mu(\mathrm{Zn\ bulk})+\Delta H_f(\mathrm{ZnO})$. Similarly, in these conditions the source of Ag is Ag_2O and $\mu(\mathrm{Ag})=\mu(\mathrm{Ag\ bulk})+(1/2)\Delta H_f(\mathrm{Ag_2O})$. The results obtained within both LDA and GGA, along with the available experimental values, are summarized in Table I. The calculated $\Delta H_f(\mathrm{Ag_2O})$ within GGA almost vanishes.[46] The calculated ΔH_f(ZnO) is in reasonable agreements with both experiment and the previous theoretical results.[26–29] In particular, the LDA and the GGA values typically bracket the experimental cohesive energies and heats of formations ΔH_f, and in most cases the accuracy of both approximations is similar.

The calculated formation energies of Ag_{Zn} are given in Table II. We see that in the Zn-rich limit the LDA and GGA values, 3.9 and 4.1 eV, respectively, are very close. A larger difference is obtained for the O-rich limit, where the GGA predicts E_{form} higher by 0.7 eV due to the large difference in the LDA and GGA values of ΔH_f(ZnO), see Table I. E_{form} obtained within the GGA in the O-rich limit, 1.2 eV, reasonably compares with 1.7 eV found in Ref. 8. As it was pointed out above, in general, the GGA and LDA results bracket the

TABLE I. Theoretical and experimental values of cohesive energies E_{coh} and heats of formation ΔH_f (in eV).

	Zn	O_2	Ag	ZnO	Ag_2O
E_{coh}(LDA)/atom	1.83	3.35	3.65	4.45	3.75
E_{coh}(GGA)/atom	1.13	3.25	2.65	3.6	2.85
E_{coh}(exp)/atom	1.35	2.6	2.95	3.75[a]	
ΔH_f(LDA)/2 atoms				−3.73	−0.4
ΔH_f(GGA)/2 atoms				−2.9	−0.05
ΔH_f(exp)/2 atoms				−3.65 [b]	

[a]Reference 1.
[b]Reference 47.

experimental data. Thus, one can expect that the actual formation energies are also bounded by the LDA and the GGA values.

To show the impact of the growth conditions on the equilibrium concentration of Ag, we assume that its formation energy is the average of the LDA and GGA values, which gives $E_{form}(Ag_{Zn})=0.85$ eV in the O-rich limit. The corresponding solubility limit, i.e., the equilibrium concentration of Ag_{Zn}, at 700 °C is about 3×10^{18} cm^{-3}. On the other hand, in the Zn-rich limit E_{form} strongly increases to 4.0 eV due to the large heat of formation of ZnO. This increase in E_{form} corresponds to a reduction in the solubility of Ag by about 10 orders of magnitude, which clearly highlights the advantageous role of the O-rich conditions for the incorporation of Ag.

The calculated LDA formation energy of Cu_{Zn} is 0.6 (3.5) eV in the O-rich (Zn-rich) limit, and the corresponding values of E_{form} for Au_{Zn} are 1.95 (5.6) eV. For the O-rich case, it is assumed that the sources of Cu and Au are, respectively, Cu_2O and Au_2O compounds. Similarly to the case of Ag_{Zn}, our LDA values are close to but somewhat lower that the GGA results obtained in Ref. 8.

We now turn to the energies of acceptor levels induced by group-I dopants. Ionization energies are given by the transition levels $\varepsilon(0/1-)$ between the neutral ($q=0$) and the negative ($q=1-$) charge states. The transition level $\varepsilon(0/1-)$ is defined as the Fermi energy at which formation energy of the neutral and the negatively charged acceptor are equal, $E_{form}(q=0)=E_{form}(q=1-)$. The formation energy of, e.g., a charged Ag_{Zn}^{1-} as a function of Fermi level E_{Fermi} is

$$E_{form}(q=1-)=E(\mathrm{ZnO:Ag}_{Zn}^{1-})-E(\mathrm{ZnO})+\mu(\mathrm{Zn})-\mu(\mathrm{Ag})+(-1)(E_V+\Delta E_{Fermi}), \quad (2)$$

where the first term on the right-hand side is the total energy of the supercell with the charged impurity. The last term represents the energy change due to the exchange of an electron between the dopant and the electron reservoir characterized by the Fermi energy $E_{Fermi}=E_V+\Delta E_{Fermi}$, where E_V is the energy of the top of the valence band of the defect-free system. From Eqs. (1) and (2) one obtains that

$$\varepsilon(0/1-)=E(\mathrm{ZnO:Ag}_{Zn}^{1-})-E(\mathrm{ZnO:Ag}_{Zn})-E_V. \quad (3)$$

The calculations were performed by following the scheme described in detail in Ref. 48. In particular, E_V was calculated in the "diluted regime," and both the potential alignment and the band filling corrections were implemented.[48] The Makov-Payne[49] image charge correction is $\Delta E_{MP}=q^2\alpha_M/2\varepsilon_0\Omega^{1/3}$ assuming point charges, where α_M is the Madelung constant, ε_0 is the static dielectric constant of ZnO, and Ω is the supercell volume. This gives $\Delta E_{MP}=0.3$ eV. However, due to the delocalized nature of the Ag_{Zn} wave function and the quadropole corrections, ΔE_{MP} is strongly reduced to about 0.05 eV, as in the case of cation vacancies in CdZnTe.[50]

According to our results obtained within GGA, Cu, Ag, and Au substituting Zn introduce $\varepsilon(0/1-)$ transition levels situated about 0.65, 0.43, and 0.55 eV above the top of the valence band, respectively. These values confirm the results obtained in Ref. 8, which are 0.7, 0.40, and 0.5 eV, respectively. Due to the hexagonal symmetry of the wurtzite structure, the acceptor level of the considered dopants is split into a singlet and a doublet which is about 0.2 eV higher in energy.

The different ionization energies of Cu, Ag, and Au may be explained by analyzing the electronic structure of acceptor levels. The decomposition of the density of states of ZnO into individual atomic orbitals, Fig. 1(a), shows that the top of the valence band is built up from ~60% of p(O) and ~40% of d(Zn) states. These states would give a dominant contribution to the wave function of a typical effective-masslike acceptor. However, as it follows from the decomposition of the density of states shown in Fig. 1(b), the Ag-induced acceptor level contains a large, about 20%,

TABLE II. Calculated formations energies (in eV) of Ag_{Zn} and of $Ag_i(+)$ in the $q=+1$ charge state assuming $E_{Fermi}=0$ and both Zn-rich and O-rich conditions.

	Zn-rich	O-rich
Ag_{Zn} (LDA)	3.9	0.5
Ag_{Zn} (GGA)	4.1	1.2
$Ag_i(+,\mathrm{GGA})$	3.0	3.0
Cu_{Zn} (LDA)	3.5	0.6
Au_{Zn} (LDA)	5.6	1.95

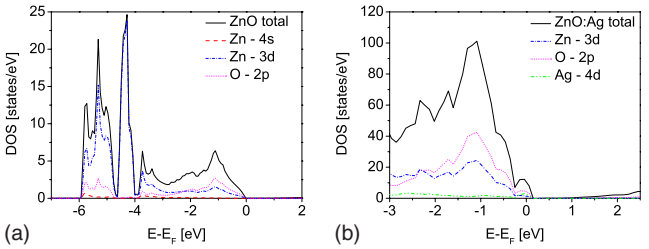

FIG. 1. (Color online) Total density of states and the contributions of the relevant atomic orbitals for (a) *w*-ZnO and (b) the Ag-induced acceptor level in the case of a 72-atom unit cell.

contribution of the *d*(Ag) orbitals, which demonstrates that a *p*(O)-*d*(Ag) hybridization takes place. Note that this contribution is higher than that of *d*(Zn). Consequently, the energies of the acceptor levels induced by Cu, Ag, and Au are partly determined by the energy of their *d* orbitals relative to the top of the valence band. In particular, Ag is the shallowest because the *d*(Ag) orbitals are the deepest and the Ag ionic radius is the largest, i.e., the hybridization causing the upward shift of the acceptor level is weaker for Ag than for Cu and Au. In agreement with this picture, the calculated outward relaxation of four oxygen neighbors of Ag by about 12% lowers the Ag acceptor energy by 0.35 eV due to the decrease in hybridization.

The low acceptor energy found for Ag shows that its potential doping efficiency is comparable to those of commonly used group-V acceptors in ZnO. Finally, the *AX*-like configuration involving a large local lattice reconstruction was shown to be metastable.[8]

Finally, we comment on the accuracy of the used approach. With the choice of parameters specified in Sec. II, formation energies are numerically converged to within 0.1 eV and energy levels to better than 0.01 eV. Thus, as it follows from the results presented in Tables I and II, the main limitation of the accuracy of E_{form} is the choice of the approximation scheme for the exchange-correlation potential, i.e., LDA or GGA. However, since formation energies are given by differences in E_{coh}, this systematic error is partially canceled, the errors in E_{form} are reduced as compared to the errors in E_{coh} and are estimated to be about 0.2–0.3 eV for neutral defects.

IV. FORMATION OF Ag_{Zn} CLUSTERS

In this section we investigate the energetics of formation of small aggregates of substitutional Ag_{Zn}. Formation of nanoinclusions involving dopants is often observed, in particular, when the dopant concentration exceeds the solubility limit. Their size and structure depend on a number of factors, and may occur either during growth or annealing. For example, in (Ga,Mn)As two types of Mn-rich clusters were observed: small clusters with the host *zb* structure and larger clusters of MnAs (Ref. 51) while in (Ga,Mn)N (Ref. 52) and ZnO:Co (Ref. 53) the inclusions are formed by metal Mn and Co nanoclusters, respectively. In ZnO:Ag, both Ag (Refs. 54 and 55) and Ag_2O (Ref. 55) phases were observed. Here, we begin with the simplest case of two acceptors, and then we add one by one consecutive Ag ions and monitor the changes in the total energy. The aggregate of four Ag ions is shown in Fig. 2.

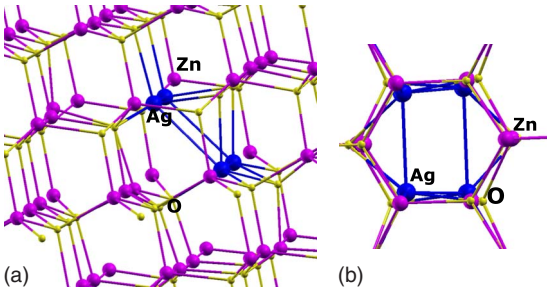

FIG. 2. (Color online) Ball-and-stick model showing a cluster of four Ag atoms, (a) side and (b) top (i.e., along the *c*-axis) view. Small (yellow), medium (magenta), and large (blue) balls represent O, Zn, and Ag atoms, respectively.

According to the obtained results, formation of a nearest-neighbor (NN) Ag_{Zn}-Ag_{Zn} pair is energetically favorable; its calculated binding energy, which is the energy of a NN pair relative to that of two isolated Ag ions, is 0.35 eV. This value is relatively large, and it implies the stability of the Ag-Ag pair at typical growth or annealing temperatures. The Ag-Ag coupling is short range since the binding of the next-nearest neighbors (NNNs) is about 10 meV.

Formation of a NN pair is reflected in the energy spectrum since the acceptor levels of the two Ag neighbors interact and form bonding and antibonding combinations. The highest state of the pair is an empty singlet, which is separated in energy by about 0.15 eV from the next singlet occupied with two electrons. Consequently, the Ag-Ag NN pair acts as a double and still shallow acceptor. Its ionization energy is higher by ~0.1 eV compared to that of an isolated Ag.

Next, we turn to the formation of an Ag_{Zn}-Ag_{Zn}-Ag_{Zn} NN triple. Formation of such a three-atom cluster is again energetically advantageous compared with the configuration of an Ag-Ag NN pair and an isolated Ag ion since the total energy of the triple is 0.1 eV lower. Note, however, that the 0.1 eV binding energy of the third Ag is weaker than that of the NN pair, 0.35 eV. Considering the electronic structure, the highest acceptor level of the triple is practically the same as that of the pair.

Finally, the formation of a cluster of four Ag_{Zn} ions confirms the tendency of Ag to aggregate: the energy gain relative to the case of NN triple and an isolated Ag is 0.45 eV, which is more than the biding energy of a pair, 0.35 eV. The energy gain relative to the configuration of four isolated Ag_{Zn} is 0.9 eV. The obtained results indicate a tendency of Ag to segregate and form *w*-AgO nanoinclusions with the wurtzite structure. As it follows from the obtained results, the segregation is partially driven by the reduction in local strains around impurities, which will be discussed in Sec. IV.

In practice, the size of Ag-rich nanoinclusions is expected to strongly depend on the efficiency of Ag diffusion, and may be kinematically suppressed or limited to clusters of a few Ag ions. This is because diffusion is typically assisted by native defects, which, in the case of Ag_{Zn}, may be Zn inter-

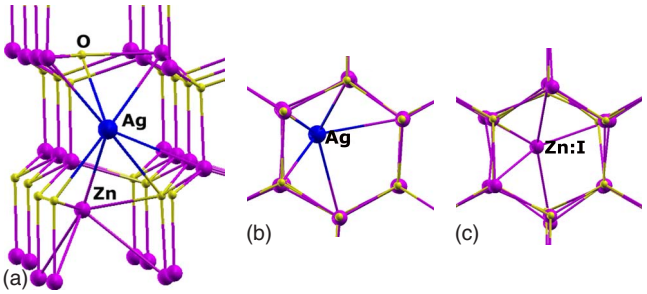

FIG. 3. (Color online) Equilibrium configuration of Ag_i. (a) side view and (b) top view. (c) Off-center configuration of the interstitial Zn. Small (yellow), medium (magenta), and large (blue) balls represent O, Zn, and Ag atoms, respectively.

stitials (for the kick-out mechanism) and/or Zn vacancies. The equilibrium concentrations of both defects in *p*-type samples and in the O-rich limit are low due to their high formation energies,[26–29] which should limit the efficiency of Ag diffusion and thus its clustering during annealing.

Summarizing, the calculations predict the formation of relatively stable Ag_{Zn} NN pairs or larger aggregates. In general, such pairs of dopant atoms in a semiconductor always exist for purely statistical reasons, i.e., even for a random distribution of impurities. The fraction of dopants that form pairs rises fast with the concentration, and becomes of importance for concentration on the order of 1%. In ZnO:Ag, the concentration of Ag-Ag pairs is expected to be higher than the statistical one. Formation of pairs and triples decreases the doping efficiency of Ag due to the increase in the ionization energies by ~0.1 eV. Larger nanoinclusions may result in the formation of *w*-AgO or other phases of silver oxide, or metal Ag.

V. INTERSTITIAL INCORPORATION OF Ag

The second mechanism that can limit the doping efficiency of Ag consists in its incorporation as an interstitial donor Ag_i, in parallel to the substitutional incorporation.[56] In the wurtzite structure, there are two high-symmetry interstitial sites, namely, the tetrahedral (I_T) and the octahedral (I_O) ones, which as a rule are local or global energy minima. For example, Zn_i in ZnO is stable at the I_O site.[26–29] Surprisingly, in the case of Ag_i these sites are local energy *maxima*. In the stable I_{C2} configuration with the C_2 symmetry, shown in Fig. 3, Ag_i is located close to the midway between two neighboring I_T and I_O sites. The very large displacements along the *c* axis of the O and Zn neighbors of Ag_i are clearly visible in Fig. 3(a). The energy of Ag_i at the I_T and I_O sites is 0.64 and 1.83 eV higher than at I_{C2}, respectively. As expected, Ag_i at I_{C2} is a single donor that may compensate Ag_{Zn}. The exact position of the Ag_i-induced level is difficult to determine given the large underestimation of the band gap within both LDA and GGA. However, with this respect we note that the recent calculations based on hybrid density functionals,[29] which provide the correct value of the band gap, show that the donor level of the Zn_i interstitial is situated above the bottom of the conduction band. A similar situation is expected for Ag_i.

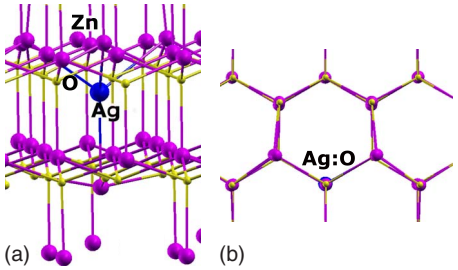

FIG. 4. (Color online) (a) Side view and (b) top view of Ag_O at the equilibrium configuration. Small (yellow), medium (magenta), and large (blue) balls represent O, Zn, and Ag atoms, respectively.

Assuming the O-rich limit and the Fermi energy at the top of the valence band, which corresponds to a *p*-type sample with Ag_{Zn} acceptors, the calculated formation energy of the positively charged Ag_i is 3.0 eV within both LDA and GGA. This is much higher than $E_{form}(Ag_{Zn})=0.85$ eV, which implies that practically all Ag atoms are incorporated as substitutional acceptors and their compensation by interstitial Ag is negligible. In Ref. 8 an even higher $E_{form}(Ag_{Zn})=4.5$ eV was obtained. The source of this discrepancy is difficult to identify given the lack of information on the location of Ag_i considered in Ref. 8 but, importantly, the main conclusion is identical.

Channeling experiments[57] show that implanted Ag in ZnO occupies two lattice sites, the substitutional one and the quasi-interstitial site that is characterized by displacements of 0.3–0.5 Å from ideal Zn sites. According to the present results, the latter case is not the equilibrium interstitial configuration with displacements larger than 1 Å shown in Fig. 3 but rather a complex with a native defect or an aggregate of Ag_{Zn} acceptors.

Finally, prompted by the results for Ag_i, we have examined the stability of a neutral Zn interstitial at the off-center I_{C2} site. We find that the configuration shown in Fig. 3(c) is a metastable local minimum with the energy higher than that of the I_O site by 50 meV only.

VI. Ag_O ANTISITE

Formation of antisite Zn_O in ZnO is characterized by an E_{form} comparable to that of Zn_i, and thus Zn_O is expected to be one of efficient compensating donor.[26–29] This suggests that also Ag may substitute for oxygen, forming an antisite-like nonintentional and quintuple acceptor. The calculated formation energies of Ag_O are 5.2 and 2.3 eV in the O-rich and O-poor conditions, respectively. These values are higher than $E_{form}(Ag_{Zn})$, mainly because of the large misfit of atomic radii of O and Ag, which induce a large relaxation around Ag_O shown in Fig. 4. Consequently, this incorporation channel is not expected to play a noticeable role, which is advantageous because Ag_O is a deeper acceptor than Ag_{Zn} and thus it should decrease the *p*-type doping efficiency by compensating the more shallow Ag_{Zn}.

VII. LATTICE CONSTANT OF ZnO:Ag

Doping of ZnO with Ag affects its lattice constant. X-ray diffraction experiments revealed that the *c* parameter of

TABLE III. Calculated lattice parameters (in Å) for *w*-ZnO and *w*-AgO.

x	*a*	*c*	*c*/*a*
ZnO	3.287	5.307	1.615
AgO	3.555	5.908	1.662

ZnO:Ag strongly depends on the conditions of growth and postgrowth annealing, and, significantly, is correlated with the type of conductivity.[13–15] Specifically, only the samples grown/annealed at "intermediate" temperatures of about 500–600 °C are *p* type, and their *c* parameter is ≈5.24 Å, which is about 0.65% larger than $c=5.207$ Å of bulk ZnO. This is in contrast to the samples grown/annealed at both "low" and "high" temperatures, which are insulating or *n* type, and have the *c* parameter ≈5.20 Å, i.e., close to that of ZnO. This dependence is indicative of differences in crystal morphology at the atomic scale. They may be caused by a number of factors related with the presence of Ag in ZnO, such as (i) incorporation or outdiffusion of substitutional Ag_{Zn}. In this case, changes in the lattice constant stem from changes in the chemical composition, and they should follow the Vegard's law, (ii) differences in distribution of Ag ions at the microscopic level, such as temperature-induced formation of Ag-rich nanoinclusions, (iii) temperature-induced annealing or generation of native defects such as V_O or Zn_i due to their increased mobilities at higher temperatures, or (iv) release of misfit strain between the substrate and the polycrystalline film. In this section we analyze the first two issues directly related with the presence of Ag.

A. Vegard's law

To find the composition dependence of the lattice parameters of *w*-(Zn,Ag)O system we begin with finding the equilibrium values for the "virtual" compound *w*-AgO in the wurtzite phase, which is not an equilibrium phase of silver oxide. The GGA results are given in Table III. In agreement with the ionic radius of Ag being larger than that of Zn, both *a* and *c* lattice parameters of *w*-AgO are larger than those of ZnO by 8.1% and 11.3%, respectively, and the *c*/*a* ratio, 1.662, is higher than the ideal value 1.633. The density of states of *w*-AgO, Fig. 5(a), shows that this virtual compound is a metal, and that the valence states are hybridized *p*(O) and *d*(Ag) orbitals. Axial distortion of *w*-AgO follows from a large contribution of *d*(Ag) orbitals parallel to the *c* axis to the bonds.

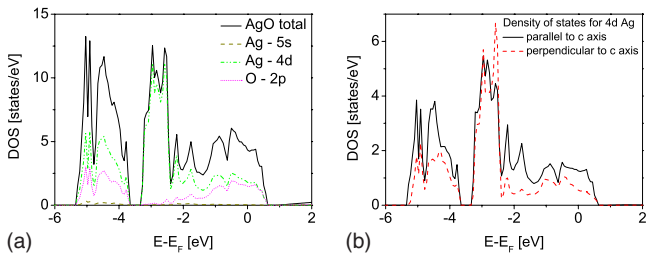

FIG. 5. (Color online) (a) Total density of states and (b) its decomposition into *d*(Ag) orbitals parallel and perpendicular to the *c* axis for *w*-AgO.

Assuming the theoretical *c* lattice constant of both ZnO and *w*-AgO and the Vegard's law, the observed increase in the *c* parameter of ZnO:Ag films by about 0.6%, i.e., from 5.207 to 5.24 Å, corresponds to ZnO containing about 6% of Ag_{Zn}, which is larger than the intentional experimental values on the order of 1%.[13–15] However, a direct comparison with experiment is not straightforward since the possible biaxial strain of ZnO epilayers would affect the *c* lattice parameter. Finally, formation of local *w*-AgO nanoclusters is expected to reduce the *c* parameter. Thus, while the effect is large and systematically observed, its origin remains to be clarified.

B. Formation of nanoinclusions

The second possible cause of the variations in the lattice constant considered in this work is the different microscopic distribution of Ag ions in the ZnO films that contain the same amount of Ag. In particular, a thermally driven redistribution of Ag during annealing at high temperatures is expected since according to the results of Sec. IV, Ag exhibits a tendency toward segregation, i.e., formation of *w*-AgO aggregates. To estimate the potential impact of segregation on the lattice constant we have compared the results for two configurations of Ag ions. In the first one, referred to as "random" in the following, the ions in the supercell are randomly distributed and distant, i.e., they do not form either NN or NNN pairs. The second configuration is that of a cluster of four NN Ag shown in Fig. 2. According to the obtained results, formation of the cluster reduces the lattice parameters by 0.007% (the *c*/*a* ratio was kept fixed in the calculations). This reduction is not an artifact of the fitting procedure because the calculated difference in total energies of the random and "cluster" configurations changes almost linearly with the lattice constants. This is expected when two total-energy quasiparabolas have minima at different *a*, and nonambiguously demonstrates the trend. However, this result has a qualitative character since the calculations were performed for a high Ag content, 6.2%, rather than for realistic Ag concentrations. On the other hand, a small aggregate of four atoms was considered while the actual size of the clusters may be much larger, which is expected to enhance the effect.

VIII. MAGNETIC PROPERTIES OF Ag ACCEPTORS

Prompted by the recent discovery of ferromagnetism in the "nominally" nonmagnetic ZnO:Cu,[58] we have examined magnetic properties of Ag in ZnO using the spin-polarized GGA approach. Spin density of an isolated Ag ion is shown in Fig. 6(a), and it corresponds to the wave function of Ag_{Zn} with an effective-masslike acceptor character. In fact, as it was pointed out in Sec. III, the highest Ag-induced acceptor level is a doublet with an appreciable contribution of *d*(Ag) orbitals. This feature is clearly seen in Fig. 6(a): the wave function is anisotropic, with a spatial extension in the (x,y) basal plane larger than that along the *c* axis. The main contributions are provided by the orbitals of Ag and of the oxy-

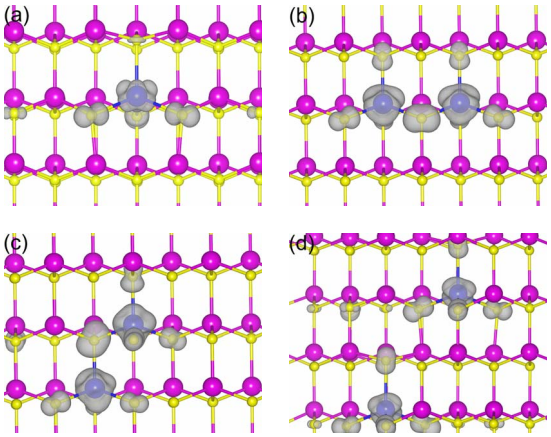

FIG. 6. (Color online) Spin density for (a) the relaxed geometry of isolated Ag, (b) for the nonrelaxed NN pair oriented in the (x,y) plane and (c) along the c axis, and (d) for the relaxed distant pair. Small (yellow), medium (magenta), and large (blue) balls represent O, Zn, and Ag atoms, respectively.

gen neighbors. More specifically, the magnetic moment of $0.25\mu_B$ is localized on the Ag ion, in agreement with Fig. 1(b) while that on each of the four oxygen nearest neighbors is $\sim 0.1\mu_B$. The spin splitting of the Ag acceptor level is ~ 0.25 eV.

The magnetic coupling between two Ag ions was examined for two nonequivalent NN pairs as well as for a "distant" pair, which are, respectively, showed in Figs. 6(b)–6(d), by calculating the difference in energies of the configurations with the parallel [ferromagnetic (FM)] and antiparallel [antiferromagnetic (AFM)] spins, $\Delta E^{\text{FM-AFM}}$. The obtained results demonstrate that the inclusion of relaxations is critical for the proper description of the coupling. In the nonrelaxed case, both NN pairs are coupled ferromagnetically, and $\Delta E^{\text{FM-AFM}}$ is -25 and -110 meV for the pair in the basal plane [Fig. 6(b)], and that oriented along the c axis [Fig. 6(c)], respectively. On the other hand, after the relaxation both the spin polarization and the magnetic coupling vanish. This result is ascribed to the effect discussed in Sec. III, where it was found that the relaxation lowers the Ag acceptor level, which both makes the wave function more delocalized thus weakening the coupling, and decreases the contribution of the d(Ag) orbital to this state. The situation is different for the distant pairs since in this case magnetization persists even after the relaxation. However, the relaxation reduces $\Delta E^{\text{FM-AFM}}$ from 65 to 18 meV. The spin-nonpolarized case is 37 meV higher in energy that the FM configuration. Thus, the coupling is qualitatively different for Ag and Cu, where the strongest coupling exists between the nearest-neighbor Cu pair.[59]

IX. SUMMARY

Properties of Ag_{Zn} acceptor in ZnO along with mechanisms limiting its doping efficiency were analyzed by first-principles calculations. Formation energies were obtained within both LDA and GGA to enhance the reliability of the results because the two approximations typically bracket the experimental data. Formation energy of Ag in the favorable O-rich conditions is ~ 0.85 eV, which corresponds to the solubility limit of about 10^{18} cm^{-3} at 700 °C. The ionization energy of Ag, ~ 0.4 eV, is relatively low, which is in agreement with experimental data[13–16] and confirms potential application of Ag as an acceptor in ZnO. On the other hand, the ionization energies of Cu and especially Au, are higher, indicating that Ag is the best group I^B species to obtain p-type ZnO. Formation energy of Cu is close to that of Ag while formation energy of Au, about 2 eV in the O-rich limit, is substantially higher. Considering the interstitial incorporation of Ag, we predict a low-symmetry equilibrium site of Ag_i that is very different from that of, e.g., interstitial Zn in ZnO. Compensation due to Ag_i donors should not be efficient due to the high formation energy of Ag_i, ~ 3 eV. Similarly, the antisite incorporation of Ag at the O sites is not expected. On the other hand, Ag reveals the tendency toward formation of AgO aggregates with the wurtzite structure, which may be efficient especially for concentrations exceeding the solubility limit. Formation of such nanoaggregates is shown to decrease the lattice constant of ZnO:Ag. The implications of this effect are discussed in the context of experimental data. Finally, magnetic coupling between Ag_{Zn} ions was investigated. Interestingly, the calculated interaction reveals an unexpected dependence on the distance between Ag ions, since the coupling between a NN pair vanishes, while it has a ferromagnetic character for more distant pairs.

ACKNOWLEDGMENTS

Part of the research was supported by the grant from the Polish Ministry of Science and Higher Education, Grant No. N50703131/0743.

[1] Ü. Özgür, Ya. I. Alivov, C. Liu, A. Teke, M. A. Reshchikov, S. Doğan, V. Avrutin, S.-J. Cho, and H. Morkoc, J. Appl. Phys. **98**, 041301 (2005).
[2] For review see, D. C. Look, J. Electron. Mater. **35**, 1299 (2006); C. Klingshirn, Phys. Status Solidi B **244**, 3027 (2007).
[3] K. K. Kim, H. S. Kim, D. K. Hwang, J. H. Lim, and S. J. Park, Appl. Phys. Lett. **83**, 63 (2003).
[4] Y. R. Ryu, S. Zhu, D. C. Look, J. M. Wrobel, H. M. Jeong, and H. W. White, J. Cryst. Growth **216**, 330 (2000).
[5] E. Przeździecka, E. Kaminska, I. Pasternak, A. Piotrowska, and J. Kossut, Phys. Rev. B **76**, 193303 (2007).
[6] F. X. Xiu, Z. Yang, L. J. Mandalapu, D. T. Zhao, and J. L. Liu, Appl. Phys. Lett. **87**, 252102 (2005).
[7] C. H. Park, S. B. Zhang, and S. H. Wei, Phys. Rev. B **66**, 073202 (2002).
[8] Y. Yan, M. M. Al-Jassim, and S.-H. Wei, Appl. Phys. Lett. **89**, 181912 (2006).
[9] Y. J. Zeng, Z. Z. Ye, J. G. Lu, W. Z. Xu, L. P. Zhu, B. H. Zhao,

and S. Limpijumnong, Appl. Phys. Lett. **89**, 042106 (2006).
[10] X. H. Wang, B. Yao, Z. P. Wei, D. Z. Sheng, Z. Z. Zhang, B. H. Li, Y. M. Lu, D. X. Zhao, J. Y. Zhang, X. W. Fan, L. X. Guan, and C. X. Cong, J. Phys. D **39**, 4568 (2006).
[11] J. G. Lu, Y. Z. Zhang, Z. Z. Ye, L. P. Zhu, L. Wang, B. H. Zhao, and Q. L. Liang, Appl. Phys. Lett. **88**, 222114 (2006).
[12] M. G. Wardle, J. P. Goss, and P. R. Briddon, Phys. Rev. B **71**, 155205 (2005).
[13] H. S. Kang, B. D. Ahn, J. H. Kim, G. H. Kim, H. W. Chang, and S. Y. Lee, Appl. Phys. Lett. **88**, 202108 (2006).
[14] R. Deng, Y. Zou, and H. Tang, Physica B **403**, 2004 (2008).
[15] L. Duan, W. Gao, R. Chen, and Z. Fu, Solid State Commun. **145**, 479 (2008).
[16] E. Kaminska, I. Pasternak, P. Boguslawski, A. Jezierski, E. Dynowska, R. Jakiela, E. Przezdziecka, A. Piotrowska, and J. Kossut, in Proceedings of the International Conference on Physics of Semiconductors (ICPS) 2008, edited by Marilia J. Caldas and Nelson Studart.
[17] Y. Kanai, Jpn. J. Appl. Phys., Part I **30**, 703 (1991).
[18] Y. Kanai, Jpn. J. Appl. Phys., Part I **30**, 2021 (1991).
[19] X. Peng, J. Xu, H. Zang, B. Wang, and Z. Wang, J. Lumin. **128**, 297 (2008).
[20] A. N. Gruzintsev, V. T. Volkov, and I. I. Khodos, Semiconductors **37**, 259 (2003).
[21] See, e.g., R. Dingle, Phys. Rev. Lett. **23**, 579 (1969); N. Y. Garces, L. Wang, L. Bai, N. C. Giles, and L. E. Halliburton, Appl. Phys. Lett. **81**, 622 (2002); M. A. Reshchikov, V. Avrutin, N. Izyumskaya, R. Shimada, H. Morkoc, and S. W. Novak, J. Vac. Sci. Technol. B **27**, 1749 (2009), and references therein.
[22] T. Ghosh, M. Dutta, S. Mridha, and D. Basak, J. Electrochem. Soc. **156**, H285 (2009).
[23] O. Schmidt, A. Geis, P. Kiesel, C. G. Van de Walle, N. M. Johnsona, A. Bakinc, A. Waag, and G. H. Döhler, Superlattices Microstruct. **39**, 8 (2006).
[24] Kwang-Soon Ahn, T. Deutsch, Yanfa Yan, C. S. Jiang, C. L. Perkins, J. Turner, and M. Al-Jassim, J. Appl. Phys. **102**, 023517 (2007); S. Shet, K.-S. Ahn, Y. Yan, T. Deutsch, K. M. Chrustowski, J. Turner, M. Al–Jassim, and N. Ravindra, *ibid.* **103**, 073504 (2008).
[25] L. J. Sun, J. Hu, H. Y. He, X. P. Wu, X. Q. Xu, B. X. Lin, Z. X. Fu, and B. C. Pan, Solid State Commun. **149**, 1663 (2009).
[26] S. B. Zhang, S. H. Wei, and A. Zunger, Phys. Rev. B **63**, 075205 (2001).
[27] A. Janotti and C. Van de Walle, J. Cryst. Growth **287**, 58 (2006).
[28] S. Lany and A. Zunger, Phys. Rev. Lett. **98**, 045501 (2007).
[29] F. Oba, A. Togo, I. Tanaka, J. Paier, and G. Kresse, Phys. Rev. B **77**, 245202 (2008).
[30] C. G. Van de Walle, Phys. Rev. Lett. **85**, 1012 (2000).
[31] P. Hohenberg and W. Kohn, Phys. Rev. **136**, B864 (1964); W. Kohn and L. J. Sham, *ibid.* **140**, A1133 (1965).
[32] J. P. Perdew, J. A. Chevary, S. H. Vosko, Koblar A. Jackson, Mark R. Pederson, D. J. Singh, and C. Fiolhais, Phys. Rev. B **46**, 6671 (1992).
[33] J. P. Perdew, K. Burke, and M. Ernzerhof, Phys. Rev. Lett. **77**, 3865 (1996).
[34] For review see, V. I. Anisimov, F. Aryasetiwan, and A. I. Lichtenstein, J. Phys.: Condens. Matter **9**, 767 (1997).
[35] A. Janotti, D. Segev. and Ch. G. Van de Walle, Phys. Rev. B **74**, 045202 (2006).
[36] N. N. Lathiotakis, A. N. Andriotis, and M. Menon, Phys. Rev. B **78**, 193311 (2008).
[37] L.-H. Ye, A. J. Freeman, and B. Delley, Phys. Rev. B **73**, 033203 (2006).
[38] www.pwscf.org
[39] G. Kresse and J. Furthmuller, Phys. Rev. B **54**, 11169 (1996).
[40] G. Kresse and D. Joubert, Phys. Rev. B **59**, 1758 (1999).
[41] D. Vanderbilt, Phys. Rev. B **41**, 7892 (1990).
[42] D. Vanderbilt, http://www.physics.rutgers.edu/~dhv/uspp/
[43] M. Methfessel and A. T. Paxton, Phys. Rev. B **40**, 3616 (1989).
[44] H. J. Monkhorst and J. D. Pack, Phys. Rev. B **13**, 5188 (1976).
[45] S. B. Zhang and J. E. Northrup, Phys. Rev. Lett. **67**, 2339 (1991).
[46] A similar value was obtained by W. X. Li, C. Stampfl, and M. Scheffler, Phys. Rev. B **67**, 045408 (2003).
[47] J. D. Cox, D. D. Wagman, and V. A. Medvedev, *CODATA Key Values for Thermodynamics* (Hemisphere, New York, 1989).
[48] C. Persson, Y. J. Zhao, S. Lany, and A. Zunger, Phys. Rev. B **72**, 035211 (2005).
[49] G. Makov and M. C. Payne, Phys. Rev. B **51**, 4014 (1995).
[50] P. Jakubas and P. Boguslawski, Phys. Rev. B **77**, 214104 (2008).
[51] M. Moreno, A. Trampert, B. Jenichen, L. Daweritz, and K. H. Ploog, J. Appl. Phys. **92**, 4672 (2002).
[52] G. Martínez-Criado, A. Somogyi, A. Homs, R. Tucoulou, and J. Susini, Appl. Phys. Lett. **87**, 061913 (2005).
[53] L. S. Dorneles, M. Venkatesan, R. Gunning, P. Stamenov, J. Alaria, M. Rooney, J. G. Lunney, and J. M. D. Coey, J. Magn. Magn. Mater. **310**, 2087 (2007).
[54] J. Xu, Z. Zhang, Y. Zhang, B. Lin, and Z. Fu, Chin. Phys. Lett. **22**, 2031 (2005).
[55] B. D. Ahn, H. S. Kang, J. H. Kim, G. H. Kim, H. W. Chang, and S. Y. Lee, J. Appl. Phys. **100**, 093701 (2006).
[56] J. Fan and R. Freer, J. Appl. Phys. **77**, 4795 (1995).
[57] U. Wahl, E. Rita, J. G. Correira, T. Agne, E. Alves, J. C. Soares, and The ISOLDE Collaboration, Superlattices Microstruct. **39**, 229 (2006).
[58] D. B. Buchholz, R. P. H. Chang, J. H. Song, and J. B. Ketterson, Appl. Phys. Lett. **87**, 082504 (2005); X. Wang, J. B. Xu, W. Y. Cheung, J. An, and N. Ke, *ibid.* **90**, 212502 (2007).
[59] L. M. Huang, A. L. Rosa, and R. Ahuja, Phys. Rev. B **74**, 075206 (2006); D. Huang, Y.-J. Zhao, D. H. Chen, and Y.-Z. Sha, Appl. Phys. Lett. **92**, 182509 (2008).